Supporting online material for

Resurgent Sodium Currents are increased in Inherited Neuronal and Muscle Channelopathies

Brian W. Jarecki[1]*, Andrew D. Piekarz[1]*, James O. Jackson II[1], Theodore R. Cummins[1]

[1]Department of Pharmacology and Toxicology, Stark Neurosciences Research Institute, Indiana University School of Medicine, Indianapolis, IN 46202, USA

* These authors contributed equally to the work. Address correspondence to T.R. Cummins; e-mail: trcummin@iupui.edu

This file includes:
Supplemental Figures 1, 2 and 3.

Supplemental Tables 1-4.

Supplemental References for Table 1

Supplemental Table 1. Sodium channelopathies that are likely to increase possibility of resurgent currents.

Mutation	Location	Syndrome	∆hinf (mV)	Persistent current	Rate of inactivation	References
Nav1.1-L263V	IS5	FHM	+8	bigger	slower	(1)
Nav1.1-T875M	IIS5-S5	GEFS+	+7	bigger	same	(2)
Nav1.1- R1648C	IV-S4	SMEI	-7	bigger	slower	(3)
Nav1.1-R1648H	IV-S4	GEFS+	-1.5	bigger	Slower	(2)
Nav1.1-F1661S	IV-S5	SMEI	+12	bigger	slower	(3)
Nav1.1-F1808L	C-term	ICEGTC	-15	bigger	same	(4)
Nav1.3-K354Q	I-S5-SS1 linker	epilepsy	-4	bigger	slower	(5)
Nav1.4-L266V	IS5	PMC/CAM	+12	same	slower	(6)
Nav1.4-V445M	IS6	PAM	-3	bigger	slower	(7)
Nav1.4-S804F	IIS6	PAM	+3	bigger	slower	(8)
Nav1.4-R1132Q	IIIS4-3	HypoPP	-4	ND	slower	(9)
Nav1.4-A1152D	IIIS4S5	PMC	+6	same	slower	(10)
Nav1.4-A1156T	IIIS4S5	PMC	+5	ND	slower	(11)
Nav1.4-G1306A	III-IV linker	PAM	+5	same	slower	(12, 13)
Nav1.4-G1306E	III-IV linker	PAM/PMC	+12	bigger	slower	(12, 13)
Nav1.4-T1313M	III-IV linker	PMC	+3/+17	same	slower	(11, 14)
Nav1.4-T1313A	III-IV linker	PMC	+11	same	slower	(15)
Nav1.4-L1433R	IVS3	PMC	+15	ND	slower	(11)
Nav1.4-R1448C/H/P/S	IVS4-1	PMC	-13	ND	slower	(11, 16-18)
Nav1.4-F1473S	IVS4S5	PAM	+18	bigger	slower	(19)
Nav1.4-F1705I	C-term	PMC	+9	ND	slower	(20)
Nav1.5-L619F	I-II linker	LQT3	+6	bigger	same	(21)
Nav1.5-S941N	II-III linker	LQT3	0	bigger	slower	(22)
Nav1.5-T1304M	IIIS4	SIDS/LQT3	+11	bigger	faster	(23)
Nav1.5-N1325S	IIIS4-S5	LQT3	ND	bigger	ND	(24)
Nav1.5-S1333Y	IIIS4-S5	SIDS/LQT3	+8	bigger	slower	(25)
Nav1.5-F1473C	III-IV linker	LQT3	+9	bigger	ND	(26)
Nav1.5-F1486L	III-IV linker	LQT3/SIDS	+14	bigger	slower	(23)
Nav1.5-∆KPQ	III-IV linker	LQT3	-6	bigger	mixed	(27)
Nav1.5-D1595H	IVS3	DCAVA	-7	bigger	slower	(28)
Nav1.5-R1623Q	IVS4	LQT3	0	bigger	slower	(29)
Nav1.5-R1626P	IVS4	LQT3	-7	bigger	slower	(22)
Nav1.5-M1652R	IVS4-S5	LQT3	+8	bigger	slower	(22)
Nav1.5-F2004L	C-term	SIDS/LQT3	+5	bigger	slower	(23)
Nav1.7-V1298F	IIIS4-S5	PEPD	+20	bigger	slower	(30)
Nav17-V1299F	IIIS4-S5	PEPD	+21	bigger	slower	(30)
Nav1.7-I1461T	IIIS4-S5	PEPD	+20	bigger	slower	(30, 31)
Nav1.7-T1464I	III-IV linker	PEPD	+19	bigger	slower	(30, 31)
Nav1.7-M1627K	IVS4-S5	PEPD	+19	bigger	slower	(31, 32)

Abbreviations: ∆hinf: change in voltage-dependence of steady-state inactivation. FHM: familial hemiplegic migraine; ICEGTC: intractable childhood epilepsy with generalized tonic-clonic seizures; SMEI: severe myoclonic epilepsy of infancy; GEFS+: generalized epilepsy with febrile seizures plus; HypoPP: hypokalemic periodic paralyis; PMC, paramyotonia congenital; PAM, potassium-aggravated myotonia; CAM, cold-aggravated myotonia; LQT3, long QT 3 syndrome; SIDS, sudden infant death syndrome; DCAVA, dilated cardiomyopathy with atrial and ventricular arrhythmia; PEPD paroxysmal extreme pain disorder; hinf, fast inactivation; c-term, c-terminus.

Supplemental Table 2. Transition rate expressions for Nav1.7 conductance simulations.

Transition	For Nav1.7	For Nav1.7-I1461T
α01	3*15.5/(1+exp((v-5)/(-12.08)))	unchanged
β01	35.2/(1+exp((v+72.7)/16.7))	unchanged
α02	2*15.5/(1+exp((v-5)/(-12.08)))	unchanged
β02	2 * (35.2/(1+exp((v+72.7)/16.7)))	unchanged
α03	15.5/(1+exp((v-5)/(-12.08)))	unchanged
β03	3 * (35.2/(1+exp((v+72.7)/16.7)))	unchanged
α11	3*15.5/(1+exp((v-5)/(-12.08)))	unchanged
β11	35.2/(1+exp((v+72.7)/16.7))	unchanged
α12	2*15.5/(1+exp((v-5)/(-12.08)))	unchanged
β12	2 * (35.2/(1+exp((v+72.7)/16.7)))	unchanged
α13	15.5/(1+exp((v-5)/(-12.08)))	unchanged
β13	3 * (35.2/(1+exp((v+72.7)/16.7)))	unchanged
αi1	-.00283+2.003/(1+exp((v+5.5266)/(-12.702)))	unchanged
βi1	0.38685/(1+exp((v+122.35)/15.29))	0.741/(1+exp((v+135.69)/21.44))
αi2	-.00283+2.003/(1+exp((v+5.5266)/(-12.702)))	1.669/(1+exp((v+10.43)/(-9.24)))
βi2	0.38685/(1+exp((v+122.35)/15.29))	0.741/(1+exp((v+135.69)/21.44))
αi3	-.00283+2.003/(1+exp((v+5.5266)/(-12.702)))	1.669/(1+exp((v+10.43)/(-9.24)))
βi3	0.38685/(1+exp((v+122.35)/15.29))	0.741/(1+exp((v+135.69)/21.44))
αi4	-.00283+2.003/(1+exp((v+5.5266)/(-12.702)))	1.05/(1+exp((v+10.43)/(-9.24)))
βi4	0.38685/(1+exp((v+122.35)/15.29))	0.9632/(1+exp((v+135.69)/21.44))
αOB	1.1*exp(v/1e12)	unchanged
βOB	0.0135*exp(v/-25)	unchanged

Transitions are as diagramed in Figure 3A. Values are in ms^{-1}.

Supplemental Table 3. Transition rate expressions for Nav1.5 conductance models.

Transition	For Nav1.5	For Nav1.5-F1486L
α01	-3*0.32*(v+47.13)/(exp(-0.1*(v+47.13))-1)	unchanged
β01	0.08 * exp(-(v)/11)	unchanged
α02	-2*0.32*(v+47.13)/(exp(-0.1*(v+47.13))-1)	unchanged
β02	2 * (0.08 * exp(-(v)/11))	unchanged
α03	-0.32*(v+47.13)/(exp(-0.1*(v+47.13))-1)	unchanged
β03	3 * (0.08 * exp(-(v)/11))	unchanged
α11	-3*0.32*(v+47.13)/(exp(-0.1*(v+47.13))-1)	unchanged
β11	0.08 * exp(-(v)/11)	unchanged
α12	-2*0.32*(v+47.13)/(exp(-0.1*(v+47.13))-1)	unchanged
β12	2 * (0.08 * exp(-(v)/11))	unchanged
α13	-0.32*(v+47.13)/(exp(-0.1*(v+47.13))-1)	unchanged
β13	3 * (0.08 * exp(-(v)/11))	unchanged
αi1	(1/(0.13*(1+(exp(-1*(v+10.66)/11.1)))))	1/(0.26*(1+(exp(-1*(v+10.66)/11.1))))
βi1	(0.135*exp(-0.147*(v+80)))	unchanged
αi2	(1/(0.13*(1+(exp(-1*(v+10.66)/11.1)))))	1/(0.26*(1+(exp(-1*(v+10.66)/11.1))))
βi2	(0.135*exp(-0.147*(v+80)))	unchanged
αi3	(1/(0.13*(1+(exp(-1*(v+10.66)/11.1)))))	1/(0.26*(1+(exp(-1*(v+10.66)/11.1))))
βi3	(0.135*exp(-0.147*(v+80)))	unchanged
αi4	(1/(0.13*(1+(exp(-1*(v+10.66)/11.1)))))	1/(0.26*(1+(exp(-1*(v+10.66)/11.1))))
βi4	(0.135*exp(-0.147*(v+80)))	0.001
αOB	2.5*exp(v/1e12)	unchanged
βOB	0.02*exp(v/-25)	unchanged

Transitions are as diagramed in Figure 3A. Values are in ms^{-1}.

Supplemental Table 4. Comparison of peak current amplitudes in cells with and without resurgent currents.

Construct	Resurgent current[1] (% of peak current)	Peak amplitude without resurgent current (nA)	Peak amplitude with resurgent current (nA)
Nav1.7r	1.0 ± 0.5 n=5 (of 21)	23.3 ± 3.7 n = 16	59.5 ± 8.3 * n = 5
Nav1.7r-I1461T	2.0 ± 0.1 n=20 (of 30)	34.9 ± 6.0 n = 10	52.7 ± 8.5 n = 20
Nav1.5	0.6 ± 0.1 n=9 (of 18)	43.9 ± 10.5 n = 9	55.1 ± 6.5 n = 9
Nav1.5-F1486L	2.0 ± 0.4 n=8 (of 17)	28.8 ± 7.9 n = 9	55.8 ± 6.0 * n = 8
Nav1.4r	None detected (out of 11)	30.9 ± 5.1 n = 11	n = 0
Nav1.4r-R1448P	4.2 ± 0.6 n=13 (of 20)	10.3 ± 1.5 n = 7	40.2 ± 4.9 * n = 13
Nav1.6r	2.4 ± 0.3 n=9 (of 14)	29.6 ± 3.1 n = 6	43.8 ± 9.6 n = 8
Nav1.6r-I1477T	15.3 ± 3.4 n=7 (of 14)	18.0 ± 3.5 n = 7	22.7 ± 2.2 n = 7

[1]Resurgent sodium current amplitude data are duplicated from Table 1 for comparison purposes. In the far right column, * indicates significant difference when comparing the peak transient current amplitude observed in cells that exhibited resurgent current to the peak transient current amplitude observed in cells that did not exhibit resurgent currents for each channel construct ($p < 0.05$).

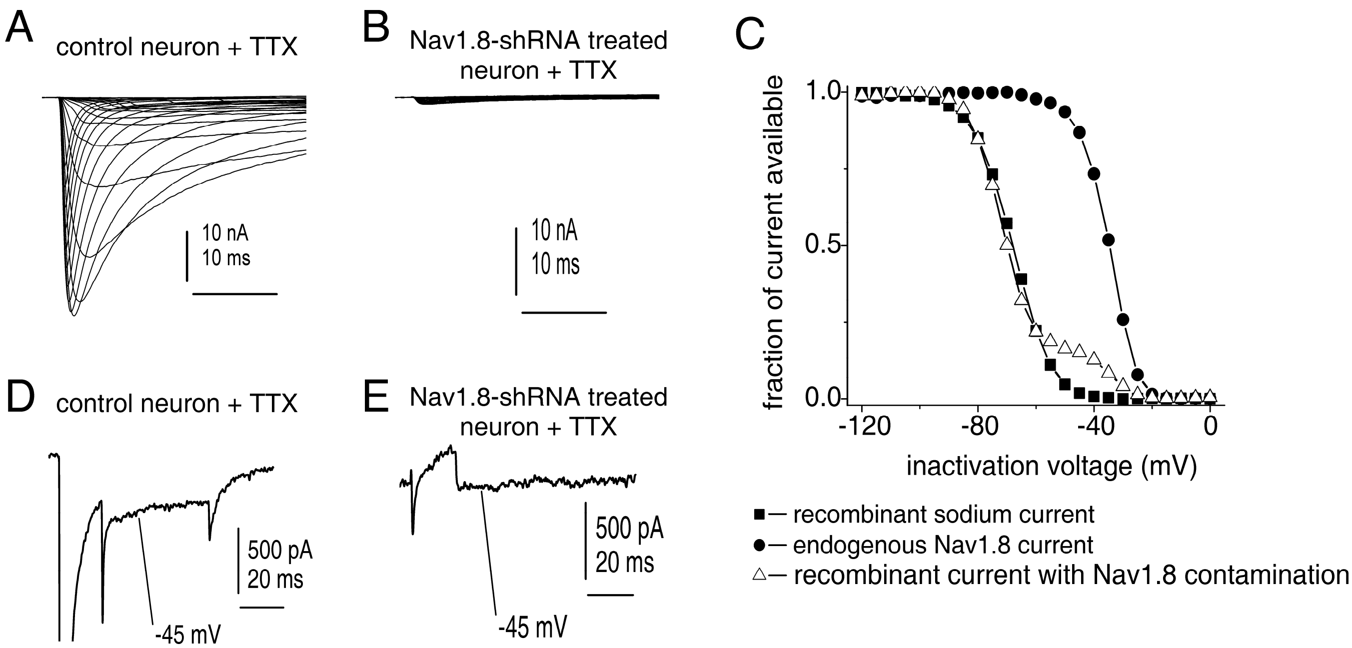

Supplemental Figure 1. (A) Representative TTX-resistant currents recorded from a cultured adult rat DRG neuron in the presence of 500 nM TTX. Currents were elicited with voltage steps ranging from -80 to +40 mV in 10 mV increments. These currents show the kinetic properties typical of Nav1.8 currents. (B) Representative currents recorded from a cultured adult rat DRG neuron transfected with Nav1.8-shRNA but no recombinant VGSC construct. Scale is the same as in (A) for comparison. In the presence of TTX, very little sodium current is elicited. This demonstrates the Nav1.8-shRNA transfection combined with application of 500 nM TTX effectively blocks the majority of endogenous voltage-gated sodium currents in cultured DRG neurons. (C) Steady-state inactivation curves for endogenous Nav1.8 currents (filled circles) recorded from the same neuron used in (A), a transfected neuron expressing recombinant Nav1.5r current without evidence of Nav1.8 contamination (closed squares) and a transfected neuron expressing recombinant Nav1.5r current with ~20% contamination by endogenous Nav1.8 currents (open triangles). Nav1.8 contamination is evidenced by the biphasic voltage-dependence of steady-state inactivation. Recordings were done in the presence of 500 nM TTX and recombinant Nav1.5r was co-transfected with Nav1.8-shRNA. (D) Resurgent currents are not detected in control neurons in the presence of 500 nM TTX. Currents are recorded from the same neuron used in (A) and are magnified 30x relative to the peak current elicited with a test pulse to -10 mV. (E) Resurgent currents are not detected in neurons transfected with Nav1.8-shRNA but no recombinant VGSC construct in the presence of 500 nM TTX. Currents are recorded from the same neuron used in (B) and are shown on the same scale as in (D) for comparison.

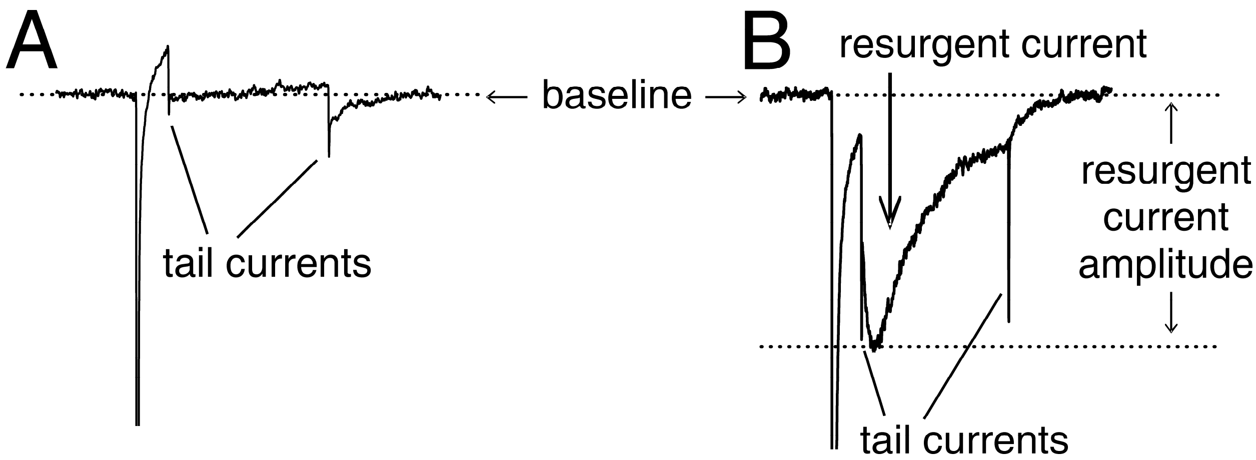

Supplemental Figure 2. Quantification of resurgent current amplitude. Sodium currents recorded from two different neurons expressing Nav1.6r currents are shown. Currents were elicited with a 20 ms pulse to +30 mV followed by a 100 ms pulse to -40 mV from a holding potential of -100 mV. Rapid tail currents can be seen in the recordings from both neurons. In addition, robust resurgent current, with slower onset and decay than the tail currents, can be seen in the recording shown in (B). The amplitude of the resurgent current is measured relative to the baseline obtained at the holding potential. Tail currents are not included in the measurement of resurgent current amplitudes through judicious use of the measurement cursors in the analysis program.

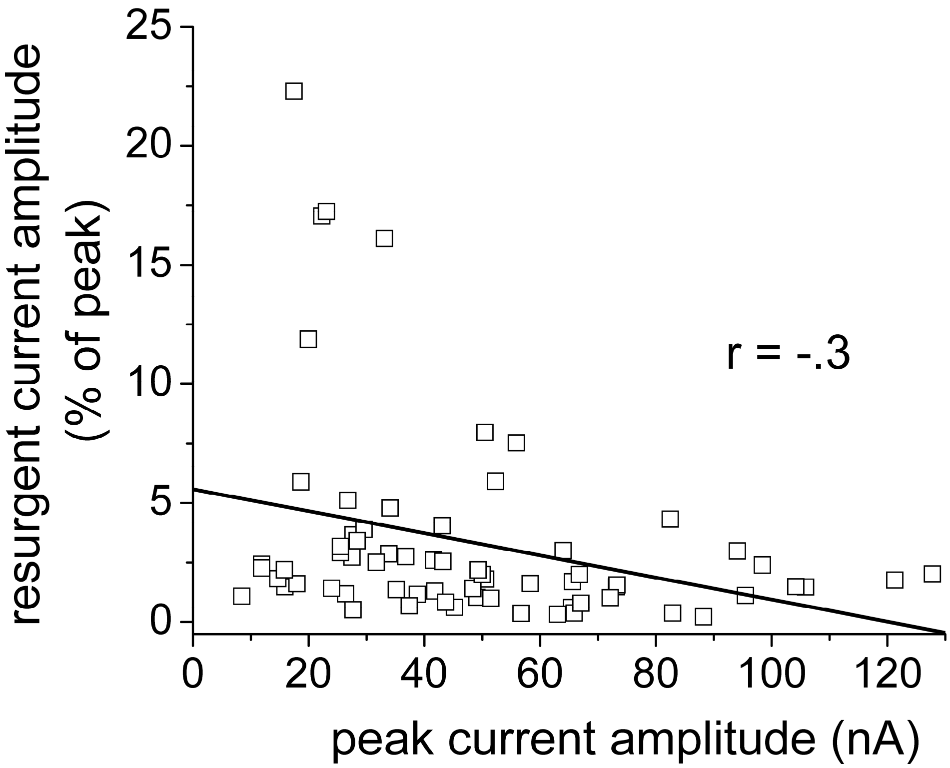

Supplemental Figure 3. Resurgent current amplitude is not well correlated with peak current amplitude. Resurgent current amplitude, expressed as a percent of peak current amplitude, is plotted versus the peak current amplitude for all 71 cells that exhibited detectable resurgent currents, regardless of channel construct. The solid line, determined using linear regression analysis, indicates that there is a slight negative correlation between resurgent current amplitude and peak current amplitude. However, this correlation is not strong, as indicated by the coefficient of correlation (r = -0.3). Furthermore, the negative slope of the fit is largely dictated by the Nav1.6r-I1477T data points; this channel exhibited large resurgent current amplitudes, but only moderate (<35 nA) peak current amplitudes. If the Nav1.6r-I1477T data points are excluded, there is virtually no correlation between peak current amplitude and the relative amplitude of the observed resurgent currents.

Supplemental References

1. Kahlig, K.M., Rhodes, T.H., Pusch, M., Freilinger, T., Pereira-Monteiro, J.M., Ferrari, M.D., van den Maagdenberg, A.M., Dichgans, M., and George, A.L., Jr. 2008. Divergent sodium channel defects in familial hemiplegic migraine. *Proc Natl Acad Sci U S A* 105:9799-9804.
2. Lossin, C., Wang, D.W., Rhodes, T.H., Vanoye, C.G., and George, A.L., Jr. 2002. Molecular basis of an inherited epilepsy. *Neuron* 34:877-884.
3. Rhodes, T.H., Lossin, C., Vanoye, C.G., Wang, D.W., and George, A.L., Jr. 2004. Noninactivating voltage-gated sodium channels in severe myoclonic epilepsy of infancy. *Proc Natl Acad Sci U S A* 101:11147-11152.
4. Rhodes, T.H., Vanoye, C.G., Ohmori, I., Ogiwara, I., Yamakawa, K., and George, A.L., Jr. 2005. Sodium channel dysfunction in intractable childhood epilepsy with generalized tonic-clonic seizures. *J Physiol* 569:433-445.
5. Holland, K.D., Kearney, J.A., Glauser, T.A., Buck, G., Keddache, M., Blankston, J.R., Glaaser, I.W., Kass, R.S., and Meisler, M.H. 2008. Mutation of sodium channel SCN3A in a patient with cryptogenic pediatric partial epilepsy. *Neurosci Lett* 433:65-70.
6. Wu, F.F., Takahashi, M.P., Pegoraro, E., Angelini, C., Colleselli, P., Cannon, S.C., and Hoffman, E.P. 2001. A new mutation in a family with cold-aggravated myotonia disrupts Na(+) channel inactivation. *Neurology* 56:878-884.
7. Wang, D.W., VanDeCarr, D., Ruben, P.C., George, A.L., Jr., and Bennett, P.B. 1999. Functional consequences of a domain 1/S6 segment sodium channel mutation associated with painful congenital myotonia. *FEBS Lett* 448:231-234.
8. Green, D.S., George, A.L., Jr., and Cannon, S.C. 1998. Human sodium channel gating defects caused by missense mutations in S6 segments associated with myotonia: S804F and V1293I. *J Physiol* 510 (Pt 3):685-694.
9. Carle, T., Lhuillier, L., Luce, S., Sternberg, D., Devuyst, O., Fontaine, B., and Tabti, N. 2006. Gating defects of a novel Na+ channel mutant causing hypokalemic periodic paralysis. *Biochem Biophys Res Commun* 348:653-661.
10. Bouhours, M., Luce, S., Sternberg, D., Willer, J.C., Fontaine, B., and Tabti, N. 2005. A1152D mutation of the Na+ channel causes paramyotonia congenita and emphasizes the role of DIII/S4-S5 linker in fast inactivation. *J Physiol* 565:415-427.
11. Yang, N., Ji, S., Zhou, M., Ptacek, L.J., Barchi, R.L., Horn, R., and George, A.L., Jr. 1994. Sodium channel mutations in paramyotonia congenita exhibit similar biophysical phenotypes in vitro. *Proc Natl Acad Sci U S A* 91:12785-12789.
12. Mitrovic, N., George, A.L., Jr., Lerche, H., Wagner, S., Fahlke, C., and Lehmann-Horn, F. 1995. Different effects on gating of three myotonia-causing mutations in the inactivation gate of the human muscle sodium channel. *J Physiol* 487 (Pt 1):107-114.
13. Groome, J.R., Fujimoto, E., and Ruben, P.C. 2005. K-aggravated myotonia mutations at residue G1306 differentially alter deactivation gating of human skeletal muscle sodium channels. *Cell Mol Neurobiol* 25:1075-1092.
14. Hayward, L.J., Brown, R.H., Jr., and Cannon, S.C. 1997. Slow inactivation differs among mutant Na channels associated with myotonia and periodic paralysis. *Biophys J* 72:1204-1219.
15. Bouhours, M., Sternberg, D., Davoine, C.S., Ferrer, X., Willer, J.C., Fontaine, B., and Tabti, N. 2004. Functional characterization and cold sensitivity of T1313A, a new mutation of the skeletal muscle sodium channel causing paramyotonia congenita in humans. *J Physiol* 554:635-647.
16. Chahine, M., George, A.L., Jr., Zhou, M., Ji, S., Sun, W., Barchi, R.L., and Horn, R. 1994. Sodium channel mutations in paramyotonia congenita uncouple inactivation from activation. *Neuron* 12:281-294.
17. Featherstone, D.E., Fujimoto, E., and Ruben, P.C. 1998. A defect in skeletal muscle sodium channel deactivation exacerbates hyperexcitability in human paramyotonia congenita. *J Physiol* 506 (Pt 3):627-638.

18. Bendahhou, S., Cummins, T.R., Kwiecinski, H., Waxman, S.G., and Ptacek, L.J. 1999. Characterization of a new sodium channel mutation at arginine 1448 associated with moderate Paramyotonia congenita in humans. *J Physiol* 518 (Pt 2):337-344.
19. Fleischhauer, R., Mitrovic, N., Deymeer, F., Lehmann-Horn, F., and Lerche, H. 1998. Effects of temperature and mexiletine on the F1473S Na+ channel mutation causing paramyotonia congenita. *Pflugers Arch* 436:757-765.
20. Wu, F.F., Gordon, E., Hoffman, E.P., and Cannon, S.C. 2005. A C-terminal skeletal muscle sodium channel mutation associated with myotonia disrupts fast inactivation. *J Physiol* 565:371-380.
21. Wehrens, X.H., Lehnart, S.E., Huang, F., Vest, J.A., Reiken, S.R., Mohler, P.J., Sun, J., Guatimosim, S., Song, L.S., Rosemblit, N., et al. 2003. FKBP12.6 deficiency and defective calcium release channel (ryanodine receptor) function linked to exercise-induced sudden cardiac death. *Cell* 113:829-840.
22. Ruan, Y., Liu, N., Bloise, R., Napolitano, C., and Priori, S.G. 2007. Gating properties of SCN5A mutations and the response to mexiletine in long-QT syndrome type 3 patients. *Circulation* 116:1137-1144.
23. Wang, D.W., Desai, R.R., Crotti, L., Arnestad, M., Insolia, R., Pedrazzini, M., Ferrandi, C., Vege, A., Rognum, T., Schwartz, P.J., et al. 2007. Cardiac sodium channel dysfunction in sudden infant death syndrome. *Circulation* 115:368-376.
24. Dumaine, R., Wang, Q., Keating, M.T., Hartmann, H.A., Schwartz, P.J., Brown, A.M., and Kirsch, G.E. 1996. Multiple mechanisms of Na+ channel--linked long-QT syndrome. *Circ Res* 78:916-924.
25. Huang, H., Millat, G., Rodriguez-Lafrasse, C., Rousson, R., Kugener, B., Chevalier, P., and Chahine, M. 2009. Biophysical characterization of a new SCN5A mutation S1333Y in a SIDS infant linked to long QT syndrome. *FEBS Lett* 583:890-896.
26. Bankston, J.R., Yue, M., Chung, W., Spyres, M., Pass, R.H., Silver, E., Sampson, K.J., and Kass, R.S. 2007. A novel and lethal de novo LQT-3 mutation in a newborn with distinct molecular pharmacology and therapeutic response. *PLoS One* 2:e1258.
27. Chandra, R., Starmer, C.F., and Grant, A.O. 1998. Multiple effects of KPQ deletion mutation on gating of human cardiac Na+ channels expressed in mammalian cells. *Am J Physiol* 274:H1643-1654.
28. Nguyen, T.P., Wang, D.W., Rhodes, T.H., and George, A.L., Jr. 2008. Divergent biophysical defects caused by mutant sodium channels in dilated cardiomyopathy with arrhythmia. *Circ Res* 102:364-371.
29. Oginosawa, Y., Nagatomo, T., Abe, H., Makita, N., Makielski, J.C., and Nakashima, Y. 2005. Intrinsic mechanism of the enhanced rate-dependent QT shortening in the R1623Q mutant of the LQT3 syndrome. *Cardiovasc Res* 65:138-147.
30. Jarecki, B.W., Sheets, P.L., Jackson, J.O., 2nd, and Cummins, T.R. 2008. Paroxysmal extreme pain disorder mutations within the D3/S4-S5 linker of Nav1.7 cause moderate destabilization of fast inactivation. *J Physiol* 586:4137-4153.
31. Fertleman, C.R., Baker, M.D., Parker, K.A., Moffatt, S., Elmslie, F.V., Abrahamsen, B., Ostman, J., Klugbauer, N., Wood, J.N., Gardiner, R.M., et al. 2006. SCN9A mutations in paroxysmal extreme pain disorder: allelic variants underlie distinct channel defects and phenotypes. *Neuron* 52:767-774.
32. Dib-Hajj, S.D., Estacion, M., Jarecki, B.W., Tyrrell, L., Fischer, T.Z., Lawden, M., Cummins, T.R., and Waxman, S.G. 2008. Paroxysmal extreme pain disorder M1627K mutation in human Nav1.7 renders DRG neurons hyperexcitable. *Mol Pain* 4:37.